IEEE Access
Multidisciplinary | Rapid Review | Open Access Journal

Received March 6, 2022, accepted March 17, 2022, date of publication March 23, 2022, date of current version April 8, 2022.

Digital Object Identifier 10.1109/ACCESS.2022.3161625

Trajectory Tracking Control of Driverless Racing Car Under Extreme Conditions

SUCAI ZHANG[1,2], GANG LI[1,2], AND LIYONG WANG[1]

[1]Beijing Key Laboratory of Measurement & Control of Mechanical and Electrical System Technology, Beijing Information Science & Technology University, Beijing 100192, China

[2]School of Automobile and Traffic Engineering, Liaoning University of Technology, Jinzhou 121001, China

Corresponding author: Gang Li (qcxyligang@lnut.edu.cn)

This work was supported by the Beijing Key Laboratory of Measurement & Control of Mechanical and Electrical System Technology, Beijing Information Science & Technology University, under Grant KF20202223201.

ABSTRACT Aiming at the problem that it is difficult to ensure the trajectory tracking accuracy and driving stability of driverless racing car under the extreme conditions of high-speed turning with different road adhesion coefficients, a trajectory tracking control strategy is proposed. Firstly, the road adhesion coefficient is estimated using the extended Kalman filter algorithm. Draw the phase plane diagram of the vehicle's centroid sideslip angle-centroid sideslip angular velocity. Use the two-line method to determine the phase plane stability area and obtain the expected limit vehicle speed under different road adhesion coefficients and different front wheel steering angle. Tracking of the desired limit travel speed is achieved through drive and brake control. Secondly, a predictive control algorithm based on adaptive prediction horizon model is designed as a lateral motion control strategy to improve the trajectory tracking accuracy. Finally, using MATLAB/Simulink and CarSim co-simulation, the results show that the proposed control strategy can ensure the driving stability of the driverless racing car and improve the trajectory tracking accuracy under extreme conditions.

INDEX TERMS Adaptive prediction horizon model predictive control, driverless racing car, extreme conditions, trajectory tracking control.

I. INTRODUCTION

In order to meet the current requirements for safe, intelligent, and efficient traffic development, and to solve problems such as environmental pollution, traffic safety and urban traffic congestion, driverless has become a hot research direction for major car companies and universities [1]. As one of the core technologies of driverless car, the motion control technology of driverless car determines all the actions performed by driverless car according to the instructions. A controller with excellent performance is the foundation of driverless technology. Since the development of driverless car control technology, the current motion control research mainly focuses on medium and low speed normal operating conditions, and trajectory tracking under extreme operating conditions is a difficult problem to be solved [2]. For driverless racing car, due to their special working conditions, driving in a track surrounded by cones of different colors, it is necessary to drive at a higher speed as much as possible without rushing out of the track limit to obtain better results. If the speed is too fast, it may be driven in the extreme working conditions of high-speed turning. Currently, it is necessary to ensure the stability and carry out the trajectory tracking control.

The common method of early research on vehicle extreme conditions control is to integrate path planning and tracking. Its advantage is that it can plan the optimal path of the vehicle in real time. However, this method has a large amount of calculation, and it is difficult to ensure real-time performance. In obtaining optimal trajectories, one approach is to generate driving trajectories through optimization algorithms. For instance, Gerdts *et al.* [3] introduced the method of optimal control and moving vision to obtain the best driving trajectory of the vehicle, so that the vehicle can track the obtained optimal trajectory. Velenis *et al.* [4] used the optimal control method to constrain the acceleration to obtain the optimal speed, thereby increasing the lap speed of the car. Cardamone *et al.* [5] decomposed the track to obtain the best cornering trajectory and used a genetic algorithm to find a balance between track length and track curvature to improve the speed of the car through corners. Some scholars also

The associate editor coordinating the review of this manuscript and approving it for publication was Shihong Ding.

use the method of simulating the technology of professional racing drivers to solve the problem of extreme conditions of vehicles. Theodosis *et al.* [6] used a set of simple curves to simulate the optimal trajectory of the vehicle during the turning process, and analyzed professional driving techniques, and concluded that the trajectory is a longer clothoid curve can improve the lap time. Casanova *et al.* [7] used a sequential quadratic programming (SQP) algorithm that minimizes functions of restricted variables to solve the resulting nonlinear programming problem to obtain the minimum vehicle maneuvering time.

In recent years, with the development of high-precision positioning technology, the simple trajectory tracking control method has gradually become the mainstream method to study the extreme conditions control of vehicles. Its characteristic is that the tracking effect has nothing to do with the path, and the control algorithm only needs to make the vehicle give full play to its own performance to obtain the optimal control effect. Therefore, many scholars focus on the control algorithm research. Bobier *et al.* [8] used the sliding mode variable structure algorithm to control the vehicle when the vehicle reached the control limit, so that the vehicle can track the trajectory quickly and smoothly. Kapania *et al.* [9] improved the trajectory tracking performance by making the direction of the vehicle's center of mass velocity the same as the tangent direction of the desired path by means of feedforward control. Erlien *et al.* [10] consider local path planning and path tracking, designed a model predictive controller for trajectory tracking control. Kapania *et al.* [11] introduced an iterative learning control algorithm to improve iterative information as transient driver input. Novi *et al.* [12] proposed a hierarchical control method based on nonlinear model predictive control (NMPC), using high-level MPC to calculate the optimal speed curve, and low-level NMPC to constrain the curve, improving the real-time performance of the control algorithm. Wang *et al.* [13] proposed a lateral control algorithm combining comprehensive feedforward-feedback and active disturbance rejection control compensation, which improved the trajectory tracking accuracy of high-speed driverless car and the robustness of the controller. Nevertheless, the control effect of the algorithm is also affected by the performance of the vehicle itself in extreme conditions. Therefore, some scholars impose constraints on vehicles to improve the control effect of the algorithm. Jin *et al.* [14] determined the vehicle limit stable car speed on the road with different adhesion coefficients and different front wheel rotation angles according to the phase plane diagram of the car's center of mass sideslip angle - the center of mass sideslip angle. Li *et al.* [15] studied the nonlinear characteristics of tires and combined tire nonlinearity with model predictive control to improve vehicle stability under extreme conditions. Chen *et al.* [16] planned the limit speed of the vehicle through the tire friction limit circle, designed a horizontal and vertical coordinated controller for trajectory tracking, and designed a stability controller to improve the driving stability of the vehicle. Xin *et al.* [17] improved the stability of the vehicle under extreme conditions by constraining the tire slip angle of the vehicle and constraining the vehicle within the stability boundary. Sun *et al.* [18] took the direction angle deviation of the velocity vector as the control reference, replaced the actual center of mass side-slip angle with the ideal center-of-mass side-slip angle, used the affine approximation method for the steering angle of the rear wheels to improve the trajectory tracking accuracy. For the vehicle extreme conditions control after the constraints are imposed, it can be regarded as solving the problem of high-order nonlinear systems with constraints, and advanced control methods can also be used. Such as BLF-based method is used to solve problems [19], [20]. A second-order sliding mode control method [21] and an adaptive SOSM controller design by using a sliding-mode-based filter [22]. The advanced control method has better control effect, considering that the driverless racing car is a very complex nonlinear system, there are different working conditions in the process of trajectory tracking. Therefore, to ensure the stability of the driverless racing car during the trajectory tracking control process as much as possible, this paper has not yet used the advanced control method in the system.

In summary, scholars have done a lot of work on the trajectory tracking control of driverless vehicle under extreme conditions. However, at present, most of the literatures focus on driverless vehicle, and there are few studies on driverless racing car. Driverless racing car have the characteristic of high-speed turning. Therefore, for the extreme conditions of high-speed turning on road with different adhesion coefficients of driverless racing car, we propose a trajectory tracking control strategy. Compared with the existing research, the main contributions include the following two aspects.

1) By plotting the phase plane of centroid sideslip angle and centroid sideslip angle velocity, the expected limit speed of the vehicle under different road adhesion coefficient and different front wheel steering angle is obtained. Compared with a fixed speed, it can better improve the stability of the vehicle under extreme conditions.
2) Based on the three degrees of freedom model of the vehicle, a linear model predictive controller is designed. According to PGC and the lateral position error, the fuzzy controller is used to adaptively control the prediction horizon of the linear model predictive controller. Compared with the fixed prediction time domain, the adaptive prediction horizon can significantly improve the trajectory tracking accuracy of the vehicle.

II. LONGITUDINAL MOTION CONTROL STRATEGY

In this article, for the trajectory tracking control of the driverless racing car under extreme conditions, it has good trajectory tracking accuracy whereas ensuring the stability of its trajectory tracking process. A trajectory tracking control strategy is proposed, as shown in Fig. 1. It mainly includes longitudinal motion control and lateral motion control.

Longitudinal motion control mainly includes road adhesion coefficient identification, stable limit vehicle speed generation, driving and braking control. Firstly, the vehicle three degrees of freedom model and the Dugoff tire model are built, and the force analysis of the vehicle model and tires is carried out to obtain the state space expression of the system, and the Kalman filter algorithm is used to estimate the road adhesion coefficient. Secondly, a simplified two degrees of freedom model is established, the phase plane diagram of centroid sideslip angle-centroid sideslip angular velocity is drawn, and the two-line method is used to determine the stable area of the phase plane, and the stable driving limit speed of different road adhesion coefficients and front wheel steering angle is obtained. According to the estimated current road adhesion coefficient and the steering angle of the front wheels of the vehicle, the stable driving limit speed of the vehicle in the current state is obtained. Drive and brake control is performed with the steady running vehicle speed as the desired vehicle speed. Lateral motion control is mainly based on the principle of model predictive control (MPC), and a linear model predictive controller is designed. According to the average of the second-order differential quotient of the road and the lateral position error, the adaptive control of the fuzzy controller is adopted for the prediction horizon of the model predictive controller. According to the difference between the current state vector of the vehicle and the reference state vector, the front wheel steering angle is solved, so that the vehicle can track the reference trajectory.

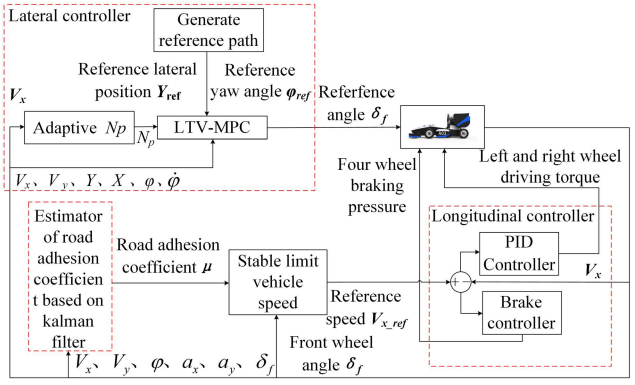

FIGURE 1. Trajectory tracking control strategy.

III. LONGITUDINAL MOTION CONTROL STRATEGY

A. DUGOFF TIRE MODEL

The Dugoff tire model is used for the tire model of the whole vehicle. Compared with other models, the Dugoff tire model can calculate the longitudinal force and lateral force through the slip rate and tire slip angle, and the road adhesion coefficient can be independent as a separate variable in the tire force, which meets the requirement of road adhesion coefficient estimation. The equations are as follows:

$$F_{x\_ij} = \mu\__{ij} F_{z\_ij} C_x \frac{\lambda\__{ij}}{1-\lambda\__{ij}} f(L) \tag{1}$$

$$F_{y\_ij} = \mu\__{ij} F_{z\_ij} C_y \frac{\tan(\alpha_{ij})}{1-\lambda\__{ij}} f(L) \tag{2}$$

where F_{x_ij} is the tire longitudinal force, F_{y_ij} is the tire lateral force, $i \in \{f, r\}$, $j \in \{l, r\}$, such as: F_{x_fl} is the longitudinal force of the left front wheel, $\mu\__{ij}$ is the road adhesion coefficient, F_{z_ij} is the tire vertical load, C_x is the longitudinal stiffness of the tire, C_y is the cornering stiffness of the tire, $\lambda\__{ij}$ is the slip rate, α_{ij} is the side slip angle of tire.

$$f(L) = \begin{cases} L(2-L), & L < 0 \\ 1, & L \geq 0 \end{cases} \tag{3}$$

where v_x is the longitudinal vehicle speed; ε is the speed influence coefficient.

The equation for calculating slip rate is:

$$\begin{cases} \lambda_{ij} = \dfrac{\omega_{ij} R_{ij}}{v_x} - 1 < 0 \ (Brake) \\ \lambda_{ij} = 1 - \dfrac{\omega_{ij} R_{ij}}{v_x} > 0 \ (Drive) \end{cases} \tag{4}$$

where ω_{ij} is the tire angular velocity; R_{ij} is the tire radius.

Normalize the tire force to get a new form:

$$F_{x\_ij} = \mu F^0_{x\_ij} = \mu F_{z\_ij} C_x \frac{\lambda\__{ij}}{1-\lambda\__{ij}} f(L) \tag{5}$$

$$F_{y\_ij} = \mu F^0_{y\_ij} = \mu F_{z\_ij} C_y \frac{\tan(\alpha\__{ij})}{1-\lambda\__{ij}} f(L) \tag{6}$$

where F^o_x is the normalized tire longitudinal force, F^0_y is the normalized tire lateral force.

B. VEHICLE ESTIMATION MODEL

The vehicle dynamic model is the basis for designing the road adhesion coefficient estimator. This section uses a three degrees of freedom dual-track dynamic model that comprehensively considers longitudinal, lateral, yaw, and longitudinal and lateral vertical load transfer, as shown in Fig. 2.

Without considering the rear wheel angle, the vehicle dynamic equations are obtained as follows:

$$\begin{aligned} a_x = \frac{1}{m}(&\mu_{fl} F^0_{x\_fl} \cos\delta_{fl} - \mu_{fl} F^0_{y\_fl} \sin\delta_{fl} \\ &+ \mu_{fr} F^0_{x\_fr} \cos\delta_{fr} - \mu_{fr} F^0_{y\_fr} \sin\delta_{fr} \\ &+ \mu_{rl} F^0_{x\_rl} + \mu_{rr} F^0_{x\_rr}) + v_y \dot{\varphi} \end{aligned} \tag{7}$$

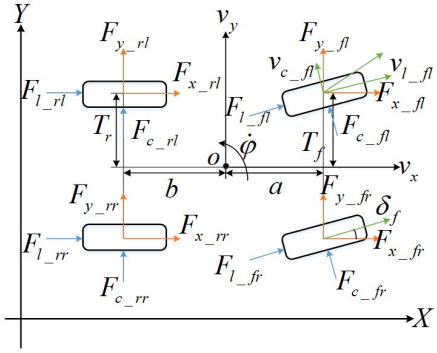

FIGURE 2. Three degrees of freedom two-rail model.

$$
\begin{aligned}
a_y = & \frac{1}{m}(\mu_{fl}F^0_{x\_fl}\sin\delta_{fl} + \mu_{fl}F^0_{y\_fl}\cos\delta_{fl} \\
& + \mu_{fr}F^0_{x\_fr}\sin\delta_{fr} + \mu_{fr}F^0_{y\_fr}\cos\delta_{fr} \\
& + \mu_{rl}F^0_{y\_rl} + \mu_{rr}F^0_{y\_rr}) - v_x\dot{\varphi} \qquad (8) \\
\ddot{\varphi} = & \frac{1}{I_z}(a(\mu_{fl}F^0_{x\_fl}\sin\delta_{fl} + \mu_{fl}F^0_{y\_fl}\cos\delta_{fl}) \\
& - \frac{T_f}{2}(\mu_{fl}F^0_{x\_fl}\cos\delta_{fl} - \mu_{fl}F^0_{y\_fl}\sin\delta_{fl}) \\
& + a(\mu_{fr}F^0_{x\_fr}\sin\delta_{fr} + \mu_{fr}F^0_{y\_fr}\cos\delta_{fr}) \\
& - \frac{T_f}{2}(\mu_{fr}F^0_{x\_fr}\cos\delta_{fr} - \mu_{fr}F^0_{y\_fr}\sin\delta_{fr}) \\
& + b\mu_{rl}F^0_{x\_rl} - \frac{T_r}{2}\mu_{rl}F^0_{x\_rl} + b\mu_{rr}F^0_{x\_rr} \\
& - \frac{T_r}{2}\mu_{rr}F^0_{x\_rr}) \qquad (9)
\end{aligned}
$$

where a_x is the longitudinal acceleration, a_y is the lateral acceleration, v_x is the longitudinal speed, v_y is the lateral speed, $\ddot{\varphi}$ is the yaw angular acceleration, m is the vehicle mass, I_z is the moment of inertia about the z-axis, T_f is the wheelbase of the front axle, T_r is the wheelbase of the rear axle, a and b are the distances between the center of mass and the front and rear axles.

The equations for calculating the vertical load of the tire are as follows:

$$F_{z\_fl} = mg\frac{b}{2l} + ma_y\frac{h_g}{T_f}\frac{b}{l} - ma_x\frac{h_g}{2l} \qquad (10)$$

$$F_{z\_fr} = mg\frac{b}{2l} - ma_y\frac{h_g}{T_f}\frac{b}{l} - ma_x\frac{h_g}{2l} \qquad (11)$$

$$F_{z\_rl} = mg\frac{b}{2l} + ma_y\frac{h_g}{T_r}\frac{b}{l} + ma_x\frac{h_g}{2l} \qquad (12)$$

$$F_{z\_rr} = mg\frac{b}{2l} - ma_y\frac{h_g}{T_r}\frac{b}{l} + ma_x\frac{h_g}{2l} \qquad (13)$$

where h_g is the height of the gravity center from the ground.

C. ROAD ADHESION COEFFICIENT ESTIMATION ALGORITHM

Based on the establishment of the vehicle model and the Dugoff normalized tire model, the extended Kalman filter algorithm is used to design a road adhesion coefficient estimator, which finally realizes the estimation of the road adhesion coefficient. The principle of the extended Kalman filter algorithm is as follows:

$$
\begin{cases}
\hat{\boldsymbol{x}}_k^- = \boldsymbol{A}\hat{\boldsymbol{x}}_{k-1} + \boldsymbol{B}u_k \\
\boldsymbol{P}_k^- = \boldsymbol{A}\boldsymbol{P}_{k-1}\boldsymbol{A}^T + \boldsymbol{Q} \\
\boldsymbol{K}_k = \dfrac{\boldsymbol{P}_k^-\boldsymbol{H}^T}{\boldsymbol{H}\boldsymbol{P}_k^-\boldsymbol{H}^T + \boldsymbol{R}} \\
\hat{\boldsymbol{x}}_k = \hat{\boldsymbol{x}}_k^- + \boldsymbol{K}_k(z_k - \boldsymbol{H}\hat{\boldsymbol{x}}_k^-) \\
\boldsymbol{P}_k = (\boldsymbol{I} - \boldsymbol{K}_k\boldsymbol{H})\boldsymbol{P}_k^-
\end{cases} \qquad (14)
$$

where $\boldsymbol{x}$ is the state vector, z is the observed vector, $\boldsymbol{A}$ is the state matrix, $\boldsymbol{B}$ is the control matrix, $\boldsymbol{u}$ is the control vector, $\boldsymbol{Q}$ is the process noise covariance matrix, $\boldsymbol{R}$ is the measurement noise covariance matrix.

Combine the vehicle dynamics equation and the normalized Dugoff tire model to determine the state vector of the system as $\boldsymbol{x}_k = \left[\mu_{fl}, \mu_{fr}, \mu_{rl}, \mu_{rr}\right]^{\mathrm{T}}$ and the observed vector as $z_k = \left[a_x, a_y, \ddot{\varphi}\right]^{\mathrm{T}}$, The system state space equations are expressed as follows:

$$\boldsymbol{x}(t) = \boldsymbol{A}x_{k-1} + \boldsymbol{Q} \qquad (15)$$

$$z_k = \boldsymbol{H}\boldsymbol{x}_k + \boldsymbol{R} \qquad (16)$$

where $\boldsymbol{A} = \begin{bmatrix} 1 & 0 & 0 & 0 \\ 0 & 1 & 0 & 0 \\ 0 & 0 & 1 & 0 \\ 0 & 0 & 0 & 1 \end{bmatrix}$, $\boldsymbol{H}$ is the Jacobian matrix of the system.

The road adhesion coefficient can be estimated by setting the initial values of the $\boldsymbol{Q}$ matrix and the $\boldsymbol{R}$ matrix in combination with the actual work conditions of the vehicle.

D. EXPECTED LIMIT DRIVING SPEED GENERATION

The complex nonlinear dynamic system of the vehicle is regarded as a controlled system, and the phase plane method is used to analyze its stability. The three degrees of freedom dynamic model of the vehicle proposed above has many parameters, so it is simplified to get nonlinear two degrees of freedom model:

$$\dot{\beta} = \frac{1}{mv_x}(F_f\cos\delta_f + F_r) - \dot{\varphi} \qquad (17)$$

$$\ddot{\varphi} = \frac{1}{I_z}(aF_f\cos\delta_f - bF_r) \qquad (18)$$

where F_f is the longitudinal force of the front tire, F_r is the longitudinal force of the rear tire.

For the above two degrees of freedom vehicle model. In a certain initial state β and $\dot{\varphi}$, the solution of the equation is a

phase trajectories start from the initial state. Choosing different initial states, multiple phase trajectories can be formed to form the phase plane of the centroid sideslip angle-yaw rate ($\beta - \dot{\varphi}$). Similarly, for different initial states β and $\dot{\beta}$, can get the phase plane of the centroid sideslip angle-the centroid sideslip angular velocity ($\beta - \dot{\beta}$). Reference [23] shows that the $\beta - \dot{\beta}$-phase plane is more suitable for vehicle stability analysis than the $\beta - \dot{\varphi}$-phase plane. Therefore, this article selects the $\beta - \dot{\beta}$-phase plane to obtain the expected limit driving speed [14].

The phase plane region is composed of multiple phase trajectories. The region of convergence and equilibrium is called the stable region, and the divergent region is called the unstable region. When the vehicle travels under different working conditions, the difference in road adhesion coefficient, front wheel angle, and driving speed will have an impact on the stable area of the $\beta - \dot{\beta}$ -phase plane. In this article, the two-line method is used to divide the stable region of the phase plane [24]. A tangent is drawn at the equilibrium points at both ends of the phase plane, and the boundary

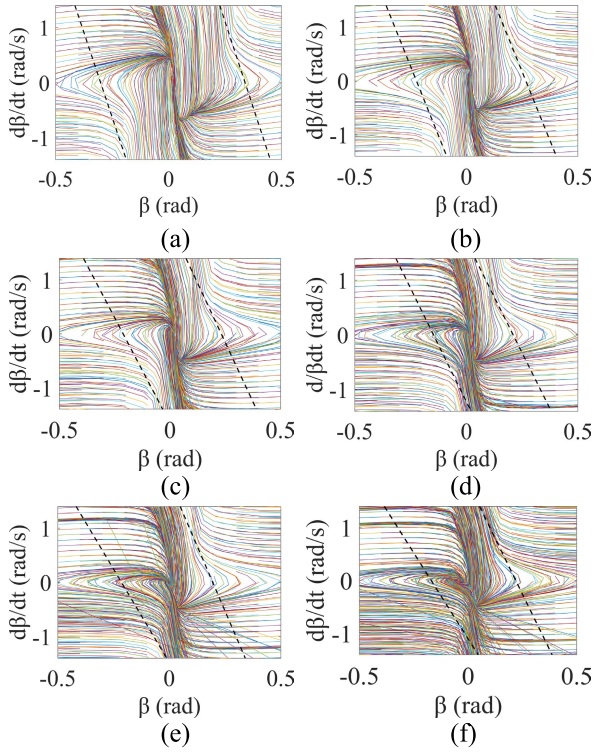

FIGURE 3. Stability boundary at different speeds: (a) $v_x = 30$km/h, (b) $v_x = 40$km/h, (c) $v_x = 50$km/h, (d) $v_x = 60$km/h, (e) $v_x = 70$km/h, (f) $v_x = 80$km/h.

equation of the stable region is:

$$\begin{cases} \dot{\beta} \geq k_1\beta + b_1 \\ \dot{\beta} \leq k_2\beta + b_2 \end{cases} \tag{19}$$

Setting the road adhesion coefficient as 0.85 and the front wheel angle as 3 degrees to obtain the stability boundary at different vehicle speeds, as shown in Fig. 3.

It can be seen from Fig. 3 that with the change of vehicle speed, the stable boundary of the phase plane changes, and the stable area of the phase plane decrease continuously.

Therefore, to obtain the limit speed of the vehicle for stable driving, by setting the road adhesion coefficient and the front wheel angle in a certain state, the vehicle speed is gradually increased to reach the boundary of the stable area. Then the vehicle speed is the expected limit vehicle speed under the current road adhesion coefficient and front wheel steering angle. Fig. 4 shows the relationship between the vehicle parameter curve and the stability boundary when the road adhesion coefficient is 0.3 and the front wheel steering angle is 3 degrees.

It can be seen from Fig. 4 (a) that when the vehicle speed is 50km/h, the vehicle parameter curve exceeds the stability boundary, and the vehicle is in an unstable state. It can be seen from Fig. 4 (b) that when the vehicle speed is reduced to 47km/h, the vehicle parameter curve is very close to the stability boundary. Therefore, under the conditions of road adhesion coefficient of 0.3 and front wheel steering angle of 3 degrees, the expected limit driving speed is 47km/h. This

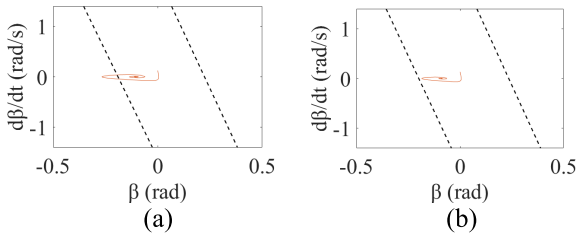

FIGURE 4. Vehicle parameter curve and stability boundariy: (a) $v_x = 50$km/h, (b) $v_x = 47$km/h.

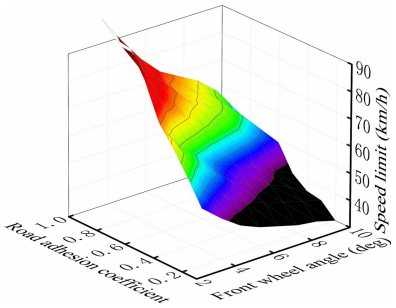

FIGURE 5. Expected limit driving speed.

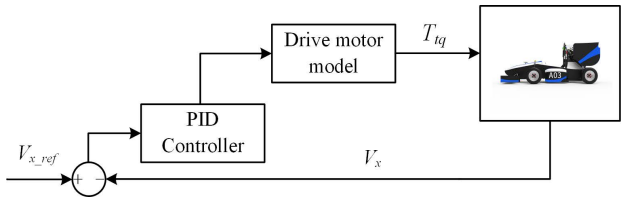

FIGURE 6. Drive control principle.

method is used to obtain the expected limit driving speed under different road adhesion coefficients and front wheel steering angle. The range of the road adhesion coefficient is: 0.2 to 0.9, the range of the front wheel steering angle is: 3° to 10°. The desired limit driving speed MAP is obtained as shown in Fig. 5.

E. DRIVE CONTROL

The driving force control uses the difference between the expected vehicle speed and the actual vehicle speed as the input of the PID controller, and outputs the motor torque to the motor model to accelerate the vehicle. The control principle is shown in Fig. 6.

F. BRAKE CONTROL

Calculate the braking deceleration according to the difference between the expected vehicle speed and the actual vehicle speed, convert the braking deceleration into braking torque, and output the braking oil pressure to decelerate the vehicle according to the relationship between the braking torque and the braking oil pressure. The control principle is shown in Fig. 7.

According to the difference between the desired vehicle speed and the current vehicle speed, the required braking

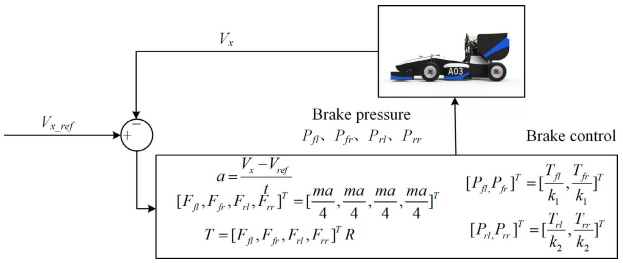

FIGURE 7. Brake control principle.

deceleration is calculated as:

$$a = \frac{v_x - v_{x\_ref}}{t} \tag{20}$$

where a is the braking deceleration, t is the braking time, and v_{x_ref} is the desired vehicle speed.

The total braking force is evenly distributed to the four wheels, and the braking torque of the four wheels is calculated as:

$$T = \frac{ma}{4}R \tag{21}$$

where T is the braking torque, R is the wheel radius.

According to the proportional relationship between the braking torque and the brake oil pressure, the braking pressure applied to the four-wheel cylinders is obtained as:

$$P_f = \frac{T}{k_1}, \quad P_r = \frac{T}{k_2} \tag{22}$$

where P_f is the braking pressure of the front wheel, P_r is the braking pressure of the rear wheel, $k_1 = 95$ is the proportional relationship of the front wheel, $k_2 = 50$ is the proportional relationship of the rear wheel.

IV. LATERAL MOTION CONTROL STRATEGY

A. VEHICLE PREDICTION MODEL

Based on the vehicle three degrees of freedom dual-track model proposed above, there are certain requirements for the real-time performance of the algorithm in the process of designing the lateral motion controller. Therefore, the model is simplified to a three degrees of freedom single-track model, as shown in Fig. 8.

Using the small angle assumption, the tire force is:

$$\begin{cases} F_{lf} = C_{lf} S_f \\ F_{lr} = C_{lr} S_r \\ F_{cf} = C_{cf}\alpha_{cf} = C_{cf}(\delta_f - \dfrac{\dot{y} + a\dot{\varphi}}{\dot{x}}) \\ F_{cr} = C_{cr}\alpha_{cr} = C_{cr}(\dfrac{b\dot{\varphi} - \dot{y}}{\dot{x}}) \end{cases} \tag{23}$$

where F_{lf} and F_{lr} is the longitudinal force of the front tire and rear tire, C_{lf} and C_{lr} is the longitudinal stiffness of the front tire and rear tire, S_f and S_r is the slip rate of the front tire and rear tire, F_{cf} and F_{cr} is the lateral force of the front tire and rear tire, C_{cf} and C_{cr} is the lateral stiffness of the front tire and rear tire, δ_f is the steering angle of front wheels, αf and αr is the tire slip angle of front and rear tire, respectively. $\dot{x}$ and $\dot{y}$ is the speed of the vehicle in the x and y axis directions, respectively.

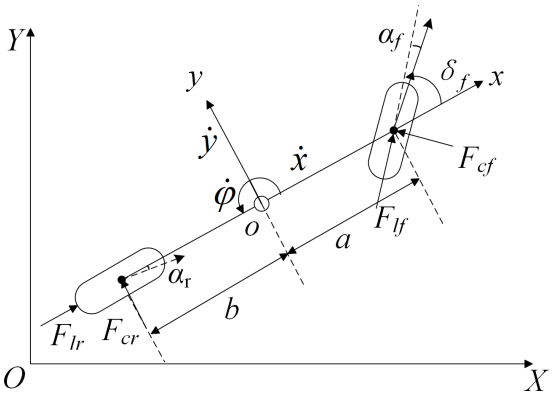

FIGURE 8. Three degrees of freedom single-track model.

According to Newton's second law, and considering the conversion between the vehicle coordinate system and the inertial coordinate system, the vehicle dynamics equation is:

$$\begin{cases} \ddot{x} = \dfrac{2}{m}[C_{lf}S_f + C_{lr}S_r - C_{cf}(\delta_f - \dfrac{\dot{y} + a\dot{\varphi}}{\dot{x}})\delta_f] + \dot{y}\dot{\varphi} \\ \ddot{y} = \dfrac{2}{m}[C_{cf}(\delta_f - \dfrac{\dot{y} + a\dot{\varphi}}{\dot{x}}) + C_{cr}\dfrac{b\dot{\varphi} - \dot{y}}{\dot{x}}] - \dot{x}\dot{\varphi} \\ \ddot{\varphi} = \dfrac{2}{I_z}[aC_{cf}(\delta_f - \dfrac{\dot{y} + a\dot{\varphi}}{\dot{x}}) - bC_{cr}\dfrac{b\dot{\varphi} - \dot{y}}{\dot{x}}] \\ \dot{Y} = \dot{x}\sin\varphi + \dot{y}\cos\varphi \\ \dot{X} = \dot{x}\cos\varphi - \dot{y}\sin\varphi \end{cases} \tag{24}$$

where $\ddot{x}$ and $\ddot{y}$ is the acceleration of the vehicle in the x and y axis directions, respectively. A and B is the speed of the vehicle in the X and Y axis directions of the inertial coordinate system, respectively.

B. MPC CONTROLLER DESIGN

The linear model predictive controller is used as the lateral motion controller. Compared with the nonlinear model predictive controller, the linear model predictive controller is relatively simple to calculate and has better real-time performance, which can meet the real-time requirements of control.

In this vehicle system, $\boldsymbol{\xi}(k) = (\dot{y}, \dot{x}, \varphi, \dot{\varphi}, Y, X)^{\mathrm{T}}$ is the system state vector and $\boldsymbol{u} = [\delta_f]$ is the control input. Convert (24) into the state space expression of the nonlinear dynamic model, perform linearization and discretization processing, and obtain the state space equation:

$$\boldsymbol{\xi}(k+1) = \boldsymbol{A}(k)\boldsymbol{\xi}(k) + \boldsymbol{B}(k)\boldsymbol{u}(k) \tag{25}$$

where $\boldsymbol{A}$(k)= $\boldsymbol{I} + T\boldsymbol{A}(t)$, $\boldsymbol{B}(k) = T\boldsymbol{B}(t)$, T is the sample period, $\boldsymbol{A}(t) = \frac{\partial f}{\partial \xi}$ is the state transition matrix, $B(t) = \frac{\partial f}{\partial u}$ is the input matrix, $\boldsymbol{I}$ is the identity matrix.

Assuming that the reference point is $(\xi_{dyn,r}, u_{dyn,r})$, derive the prediction equation of MPC and convert (25) into the form of augmented matrix.

$$\boldsymbol{\xi}(k|k) = \begin{bmatrix} \tilde{\boldsymbol{x}}(k|k) \\ \tilde{\boldsymbol{u}}(k-1|k) \end{bmatrix} \tag{26}$$

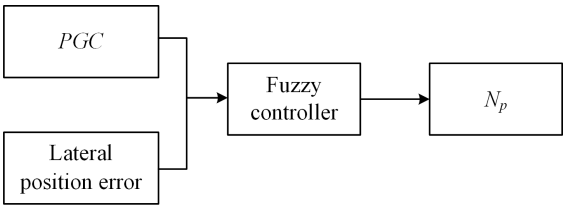

FIGURE 9. Adaptive prediction horizon adjustment.

where $\tilde{\boldsymbol{x}}(k\,|k) = \boldsymbol{\xi}(k) - \boldsymbol{\xi}_{dyn,r}(k)$, $\tilde{\boldsymbol{u}}(k-1\,|k) = \boldsymbol{u}(k-1) - \boldsymbol{u}_{\boldsymbol{dyn},\boldsymbol{r}}(k-1)$.

A new equation can be written as

$$\begin{aligned}\boldsymbol{\xi}(k+1|k) &= \tilde{\boldsymbol{A}}(k)\boldsymbol{\xi}(k|k) + \tilde{\boldsymbol{B}}(k)\Delta\boldsymbol{u}(k|k)\\ \boldsymbol{\eta}(k|k) &= \tilde{\boldsymbol{C}}(k)\boldsymbol{\xi}(k|k)\end{aligned} \tag{27}$$

where

$$\tilde{\boldsymbol{A}}(k) = \begin{bmatrix}\boldsymbol{A}(k) & \boldsymbol{B}(k)\\ \boldsymbol{0}_{1\times 6} & \boldsymbol{I}_1\end{bmatrix},\quad \tilde{\boldsymbol{B}}(k) = \begin{bmatrix}\boldsymbol{B}(k)\\ \boldsymbol{I}_1\end{bmatrix},$$
$$\tilde{\boldsymbol{C}}(k) = \begin{bmatrix}0 & 0 & 1 & 0 & 0 & 0\\ 0 & 0 & 0 & 0 & 1 & 0\end{bmatrix}.$$

According to (27), the model prediction equation of the k sample time can be expressed as

$$\boldsymbol{Y}(k+1|k) = \boldsymbol{\psi}\boldsymbol{\xi}(k) + \boldsymbol{\Theta}\Delta\boldsymbol{U}(k) \tag{28}$$

where $\boldsymbol{Y}(k+1|k)$ is the system output at the k sample time, $\Delta\boldsymbol{U}(k)$ is the system input at the k sample time, $\boldsymbol{Y}(k+1|k)$, $\Delta\boldsymbol{U}(t)$, $\boldsymbol{\Theta}$, and $\boldsymbol{\psi}$, as shown at the bottom of the next page, N_p is the prediction horizon, N_c is the control horizon.

The cost function is designed as:

$$\begin{aligned}\boldsymbol{J} = \sum_{i=1}^{N_p} ||\eta(k+i|k) - \boldsymbol{\eta}_{\text{ref}}(k+i|k)||_{\boldsymbol{Q}}^2\\ + \sum_{i=1}^{N_c-1} ||\Delta\boldsymbol{u}(k+i|k)||_{\boldsymbol{R}}^2 + \rho\varepsilon^2\end{aligned} \tag{29}$$

where $\boldsymbol{\eta}(k+i|k)$ is the actual system state, $\boldsymbol{\eta}_{ref}(k+i|k)$ is the referenced system state, $\Delta u(k+i|k)$ is the control increment of the front wheel steering angle, $\boldsymbol{Q}$ is the state weight coefficient matrix, $\boldsymbol{R}$ is the control increment weight coefficient matrix, ρ is the relaxation factor weight coefficient, ε is the relaxation factor.

The constraint of the front wheel steering angle and the variation are designed as

$$\begin{bmatrix}-20^\circ \le \delta_f \le 20^\circ\\ -0.85^\circ \le \Delta\delta_f \le 0.85^\circ\end{bmatrix} \tag{30}$$

Solving the following constrained optimization problem to obtain the optimal control increment acting on the system

$$\begin{cases}\min\ J\\ \Delta\boldsymbol{U}_{\min} \le \Delta\boldsymbol{U}_t \le \Delta\boldsymbol{U}_{\max}\\ \boldsymbol{U}_{\min} \le \boldsymbol{U}_t \le \boldsymbol{U}_{\max}\\ \boldsymbol{y}_{hc,\min} \le \boldsymbol{y}_{hc} \le \boldsymbol{y}_{hc,\max}\\ \boldsymbol{y}_{sc,\min} - \varepsilon \le \boldsymbol{y}_{sc} \le \boldsymbol{y}_{sc,\max} + \varepsilon\end{cases} \tag{31}$$

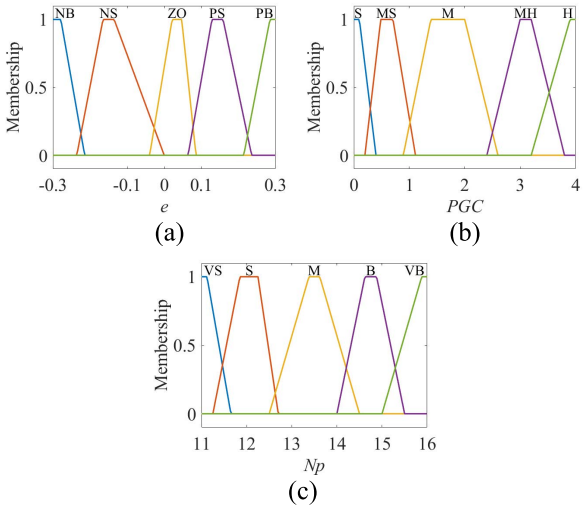

FIGURE 10. Membership function: (a) membership function of e, (b) membership function of *PGC*, (c) membership function of N_p.

TABLE 1. Fuzzy rule control table.

		PGC				
		S	MS	M	MH	H
	NB	VS	B	VB	VB	VB
	NS	M	M	VB	VB	B
e	ZO	S	S	B	B	M
	PS	M	M	VB	VB	B
	PB	VS	B	VB	VB	VB

TABLE 2. Vehicle parameters.

Symbol	Parameters	Value and units
m	Vehicle mass	260 kg
a	Distance from vehicle gravity center to the front axle	0.7605 m
b	Distance from vehicle gravity center to the rear axle	0.8095 m
R	Effective radius of wheel	0.26 m
l	Wheelbase of vehicle	1.57 m
T_f	Wheelbase of the front axle	1.2 m
T_r	Wheelbase of the rear axle	1.18 m
h_g	The height of the gravity center	0.3 m

where $\Delta\boldsymbol{U}_{\min}$ and $\Delta\boldsymbol{U}_{\max}$ are the minimum and maximum values of the control input increment, $\boldsymbol{U}_{\min}$ and $\boldsymbol{U}_{\max}$ are the minimum and maximum values of the control input, $\boldsymbol{y}_{hc,\min}$ and $\boldsymbol{y}_{hc,\max}$ are the minimum and maximum values of the hard constraint of output, $\boldsymbol{y}_{sc,\min}$ and $\boldsymbol{y}_{sc,\max}$ are the minimum and maximum values of the soft constraint of output.

TABLE 3. Controller parameters.

Parameters	A	B	C	D
Prediction horizon	Adaptive	16	11	16
Control horizon	9	9	9	9
Sample period	0.01	0.01	0.01	0.01
Weight coefficient matrix $\boldsymbol{Q}$	$Q = diag$[5000, 20000]	$Q = diag$[5000, 20000]	$Q = diag$[5000, 20000]	$Q = diag$[5000, 20000]
Speed	Variable speed	Variable speed	Variable speed	Constant speed

Solving (24), the optimal front wheel steering angle increment sequence is obtained as follows:

$$\Delta \boldsymbol{U}_t^* = \left[\Delta \boldsymbol{u}_t^*, \Delta \boldsymbol{u}_{t+1}^*, \cdots, \Delta \boldsymbol{u}_{t+N_c-1}^*, \varepsilon\right]^{\mathrm{T}} \tag{32}$$

The first item of the increment sequence is used as the control increment input of the system.

$$\boldsymbol{u}(t) = \boldsymbol{u}(t-1) + \Delta \boldsymbol{u}_t^* \tag{33}$$

C. ADAPTIVE PREDICTION HORIZON

The prediction horizon N_p is one of the main parameters affecting the control effect of the MPC controller. Therefore, this article uses a fuzzy controller to adaptively control the prediction horizon N_p to improve the control accuracy of the controller.

Firstly, the average of the absolute value of the second derivative of the road is introduced to define the lateral position change of the reference path [25], as follows:

$$PGC = \frac{1}{N_p - 1}\left(\sum_{j-1}^{N_p-1} \left|f''(x_{r,j+1})\right|\right) \tag{34}$$

Where $f''(x_{r,j+1}) = \frac{f'(x_{r,j+1}) - f'(x_{r,j})}{\Delta x_r}$, $\Delta x_{r,j} = (j-1)\Delta x_r$, $f'(x_{r,j+1}) = \frac{f(x_{r,j+1}) - f(x_{r,j})}{\Delta x_r}$, $\Delta x_r = v_x T$, T is the sample time, j is an integer between 1 to $N_p + 1$.

The prediction horizon N_p represents the prediction step size of the system for the future time. If N_p is larger, the characteristic of the system is that it cares more about the state of the future moment, and the weight of the state of the current moment is smaller. Therefore, the control effect shown is that the control accuracy of the current state is reduced, but the stability of the control system is better. On the contrary, the characteristic of the system is that the more it cares about the state of the current moment, the less weight it gives to the state of the future moment. Therefore, the control effect shown is that the control accuracy of the current moment is better, but the stability of the control system is deteriorated due to the small prediction of the future moment. Therefore, the reasonable choice of prediction horizon N_p has a very important influence on the control results [26]. The vehicle state of the driverless racing car changes during the trajectory tracking process, and the fixed prediction horizon cannot guarantee the optimal control effect in different states.

Based on the above principles, to ensure the stability of the vehicle and at the same time improve the trajectory tracking accuracy in different vehicle states. According to *PGC* and lateral position error, the prediction horizon N_p is adaptively adjusted using a fuzzy controller. Fixed control horizon N_c is adopted. The adaptive prediction horizon adjustment control structure is shown in Fig. 9.

$$\boldsymbol{Y}(k+1|k) = \begin{bmatrix} \boldsymbol{\eta}(k+1|k) \\ \boldsymbol{\eta}(k+2|k) \\ \cdots\cdot \\ \boldsymbol{\eta}(k+N_p|k) \end{bmatrix}, \quad \Delta \boldsymbol{U}(t) = \begin{bmatrix} \Delta \boldsymbol{u}(k) \\ \Delta \boldsymbol{u}(k+1) \\ \cdots\cdot\cdot \\ \Delta \boldsymbol{u}(k+N_c-1) \end{bmatrix}$$

$$\boldsymbol{\Theta} = \begin{bmatrix} \tilde{\boldsymbol{C}}(k)\tilde{\boldsymbol{B}}(k) & \boldsymbol{0} & \boldsymbol{0} & \boldsymbol{0} \\ \tilde{\boldsymbol{C}}(k)\tilde{\boldsymbol{A}}(k)\tilde{\boldsymbol{B}}(k) & \tilde{\boldsymbol{C}}(k)\tilde{\boldsymbol{B}}(k) & \boldsymbol{0} & \boldsymbol{0} \\ \tilde{\boldsymbol{C}}(k)\tilde{\boldsymbol{A}}_{t,t}^2\tilde{\boldsymbol{B}}(k) & \tilde{\boldsymbol{C}}(k)\tilde{\boldsymbol{A}}(k)\tilde{\boldsymbol{B}}(k) & \tilde{\boldsymbol{C}}(k)\tilde{\boldsymbol{B}}(k) & \boldsymbol{0} \\ \cdots\cdot & \tilde{\boldsymbol{C}}(k)\tilde{\boldsymbol{A}}^2(k)\tilde{\boldsymbol{B}}(k) & \tilde{\boldsymbol{C}}(k)\tilde{\boldsymbol{A}}(k)\tilde{\boldsymbol{B}}(k) & \tilde{\boldsymbol{C}}(k)\tilde{\boldsymbol{B}}(k) \\ \tilde{\boldsymbol{C}}(k)\tilde{\boldsymbol{A}}^{N_p-2}(k)\tilde{\boldsymbol{B}}(k) & \cdots & .. & .. \\ \tilde{\boldsymbol{C}}(k)\tilde{\boldsymbol{A}}^{N_p-1}(k)\tilde{\boldsymbol{B}}(k) & \tilde{\boldsymbol{C}}(k)\tilde{\boldsymbol{A}}^{N_p-2}(k)\tilde{\boldsymbol{B}}(k) & \cdots\cdot & \tilde{\boldsymbol{C}}(k)\tilde{\boldsymbol{A}}^{N_p-N_c-1}(k)\tilde{\boldsymbol{B}}(k) \end{bmatrix}$$

$$\boldsymbol{\psi} = \begin{bmatrix} \tilde{\boldsymbol{C}}(k)\tilde{\boldsymbol{A}}(k) \\ \tilde{\boldsymbol{C}}(k)\tilde{\boldsymbol{A}}^2(k) \\ \cdots\cdot \\ \tilde{\boldsymbol{C}}(k)\tilde{\boldsymbol{A}}^{N_p}(k) \end{bmatrix},$$

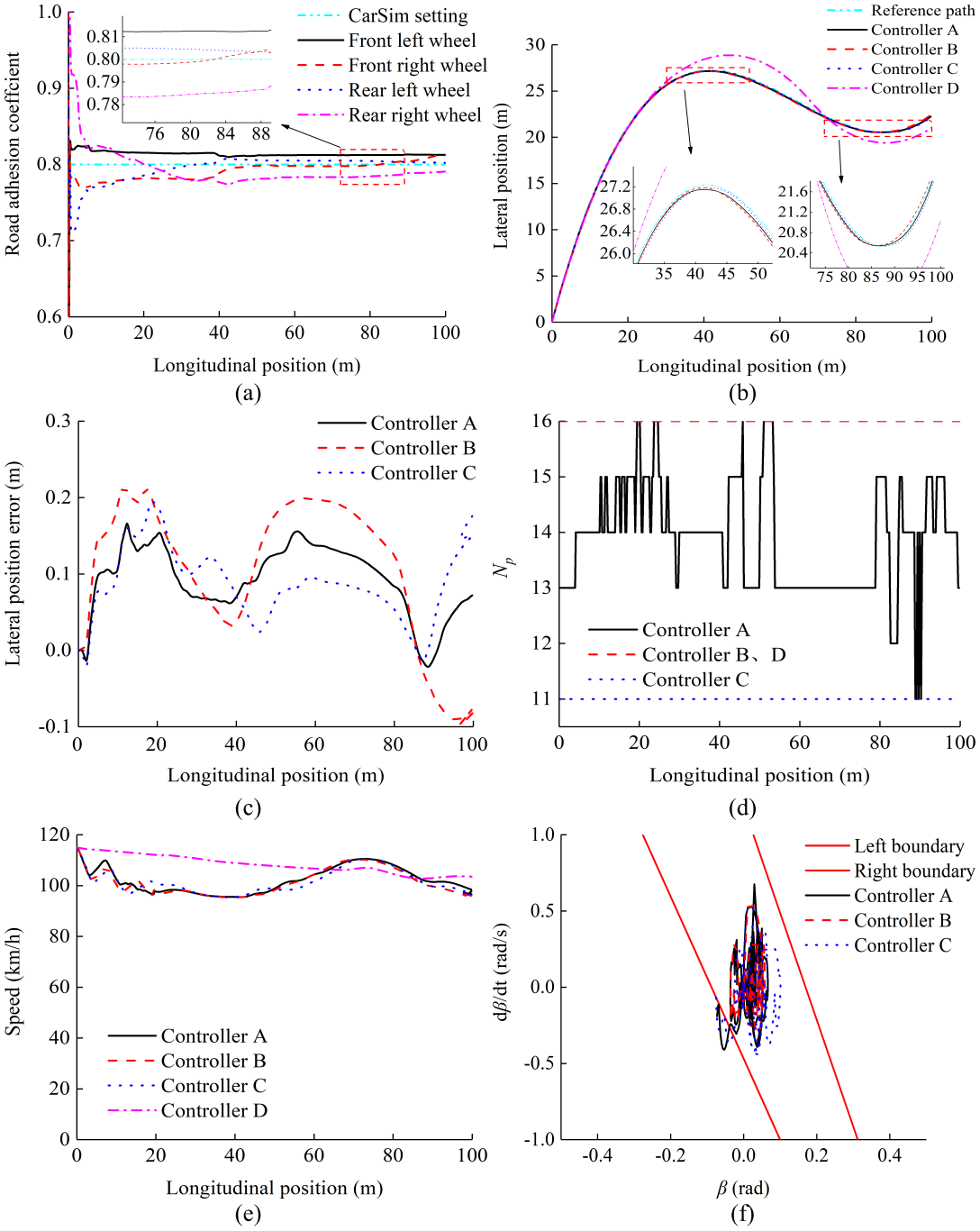

FIGURE 11. Simulation results of high adhesion coefficient road: (a) the estimation result of road adhesion coefficient, (b) the comparison of vehicle trajectory, (c) the comparison of lateral position error, (d) the comparison of prediction horizon, (e) the comparison of speed, (f) phase plane.

Define the fuzzy domain of PGC is {0,1,2,3,4}. The corresponding fuzzy subset is {S,MS,M,MH,H}. The fuzzy domain of lateral position error is {−0.3, −0.15, 0, 0.15, 0.3}. The corresponding fuzzy subset is {NB,NS,ZO,PS,PB}. The basic domain corresponding to the output N_p is [11], [16], the fuzzy domain is {1,1.25,1.5,1.75,2}, the corresponding fuzzy subset is {VS,S,M,B,VB}. The input and output membership functions are all trapezoidal functions, as shown in Fig. 10. The fuzzy rule control table is shown in Table. 1.

V. SIMULATION RESULTS

The controller is built in MATLAB/Simulink, the vehicle model is built in CarSim, and the co-simulation is carried out to verify the proposed control strategy. The main parameters of the vehicle are shown in Table. 2.

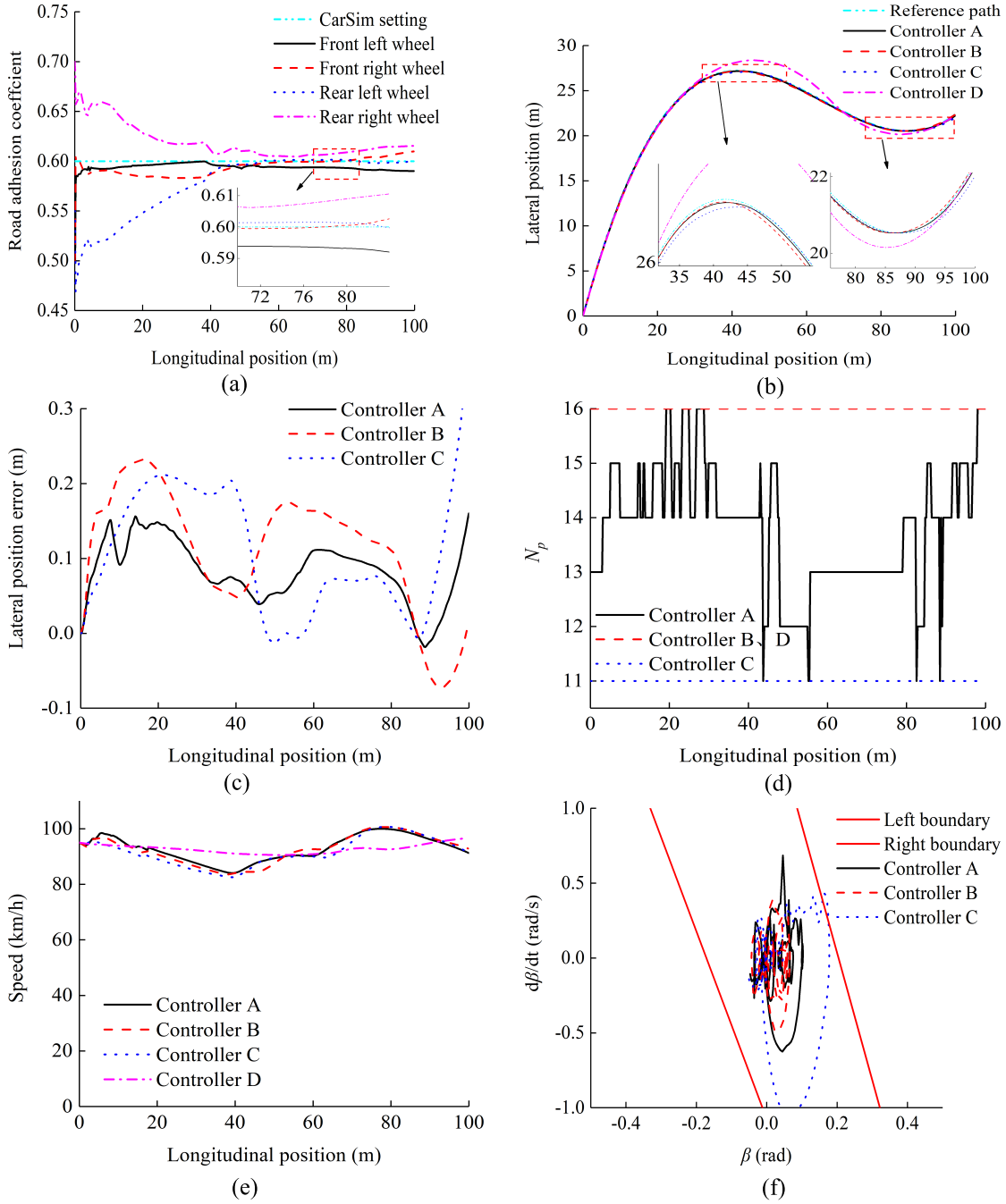

FIGURE 12. Simulation results of medium adhesion coefficient road: (a) the estimation result of road adhesion coefficient, (b) the comparison of vehicle trajectory, (c) the comparison of lateral position error, (d) the comparison of prediction horizon, (e) the comparison of speed, (f) phase plane.

Considering that the path of the driverless racing competition is a combination of straights and corners, it is to verify the trajectory tracking control under the extreme conditions of high-speed turning. Therefore, a simulation path is established by cubic spline curve fitting. Its reference path and reference yaw angle are shown as follows:

$$\begin{aligned} Y_{ref}(X) &= aX^3 + bX^2 + cX + d \\ \varphi_{ref}(X) &= 3aX^2 + 2bX + c \end{aligned} \tag{35}$$

where Y_{ref} is the reference lateral position, X is the longitudinal position, φ_{ref} is the reference yaw angle, $a = 0.0001422$, $b = -0.02751$, $c = 1.553$, $d = 0$.

In the simulation environment, the initial position of the vehicle in the geodetic coordinate system is set to (0,0), and the initial yaw angle is 57.3°. Set up four groups of controllers for comparison, namely: controller A, controller B, controller C, and controller D. Controller A is an adaptive prediction horizon model predictive controller. Controller B

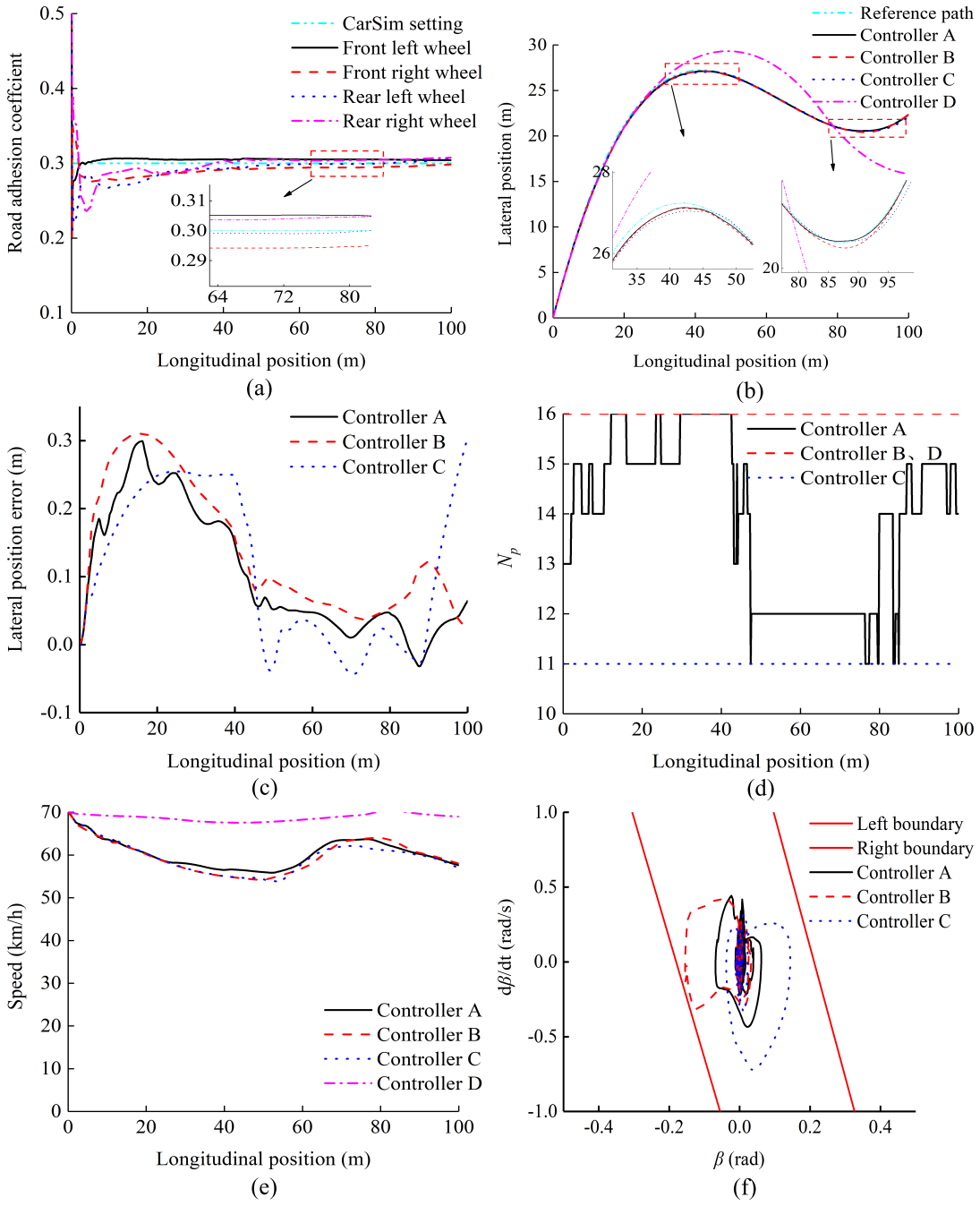

FIGURE 13. Simulation results of low adhesion coefficient road: (a) the estimation result of road adhesion coefficient, (b) the comparison of vehicle trajectory, (c) the comparison of lateral position error, (d) the comparison of prediction horizon, (e) the comparison of speed, (f) phase plane.

is a fixed prediction horizon model predictive controller ($N_p = 16$). Controller C is a fixed prediction horizon model predictive controller ($N_p = 11$). Controller D is a constant longitudinal vehicle speed, fixed prediction horizon model predictive controller ($N_p = 16$). The vehicle speed of controllers A, B, and C are controlled by the longitudinal motion control strategy designed in this article. The controller parameters are shown in Table. 3.

A. CASE STUDY 1: HIGH ADHESION COEFFICIENT ROAD

The road adhesion coefficient is set to 0.8 and the initial vehicle speed is 115 km/h. The simulation results are shown in Fig. 11.

As can be seen from Fig. 11 (a)-(f), after 28 m, the entry into the curve starts at this time. Controller D cannot accurately track the trajectory because the vehicle speed is too fast, and the vehicle has a large deviation from the

reference trajectory. The other three sets of controllers decelerate according to the front wheel steering angle, and the speed is almost the same, which can track the trajectory stably and accurately. The maximum lateral position error of controller B is 0.21 m. The maximum lateral position error of controller A is 0.15 m. The maximum lateral position error of controller C is 0.2 m. Compared with fixed prediction horizon; adaptive prediction horizon control can effectively improve the accuracy of trajectory tracking control. The road adhesion coefficient estimator has small fluctuations in the estimation process, and finally converges around the set value of 0.8. The maximum estimation error of the road adhesion coefficient is 0.03, which has a good estimation effect. The vehicle speed of 95 km/h at the longitudinal position of 35m-50m is selected as the boundary of the centroid sideslip angle - the centroid sideslip angular velocity phase plane. Only a small part of the vehicle's own trajectory curve of the three controllers exceeds the boundary curve, and the vehicle is in a stable state. Therefore, on the road with high adhesion coefficient, the proposed trajectory tracking control strategy has a better trajectory tracking control effect under extreme conditions.

B. CASE STUDY 2: MEDIUM ADHESION COEFFICIENT ROAD

The road adhesion coefficient is set to 0.6 and the initial vehicle speed is 95 km/h. The simulation results are shown in Fig. 12.

As can be seen from Fig. 12 (a)-(f), after 28 m, the entry into the curve starts at this time. Controller D cannot accurately track the trajectory because the vehicle speed is too fast, and the vehicle has a large deviation from the reference trajectory. But after the longitudinal position of 70m, since the curvature of the curve is smaller than that of the first curve, the controller D can continue to track the trajectory. The other three sets of controllers decelerate according to the front wheel steering angle, and the speed is almost the same, which can track the trajectory stably and accurately. The maximum lateral position error of controller B is 0.22 m. The maximum lateral position error of controller A is 0.15 m. The maximum lateral position error of controller C is 0.2 m. However, after 90m, due to the small prediction horizon, the lateral position error of the exit increases, and the maximum is 0.4m. The road adhesion coefficient estimator has small fluctuations in the estimation process, and finally converges around the set value of 0.6. The maximum estimation error of the road adhesion coefficient is 0.02, which has a good estimation effect. The vehicle speed of 85 km/h at the longitudinal position of 35m-50m is selected as the boundary of the centroid sideslip angle - the centroid sideslip angular velocity phase plane. The vehicle trajectory curves of the three groups of controllers are almost all within the boundary curve, and the vehicle is in a stable state. Therefore, the proposed trajectory tracking control strategy also has a good trajectory tracking control effect under the medium adhesion coefficient road surface.

C. CASE STUDY 3: LOW ADHESION COEFFICIENT ROAD

The road adhesion coefficient is set to 0.3 and the initial vehicle speed is 70 km/h. The simulation results are shown in Fig. 13.

As can be seen from Fig. 13 (a)-(f), after 28 m, the entry into the curve starts at this time. Controller D cannot accurately track the trajectory because the vehicle speed is too fast, and the vehicle has a large deviation from the reference trajectory. The other three sets of controllers decelerate according to the front wheel steering angle, and the speed is almost the same, which can track the trajectory stably and accurately. Due to the low adhesion coefficient of the road surface, compared with the previous two working conditions, the lateral position error of controller D exceeds 3 m, and the trajectory tracking cannot be continued. The maximum lateral position error of controller B is 0.3m. The maximum lateral position error of controller A is 0.3m. Before the longitudinal position of 90m, the maximum lateral position error of controller C is 0.25m. However, after 90m, due to the small road adhesion coefficient and the small prediction horizon, the lateral position error of the exit increases to 0.3m. The road adhesion coefficient estimator has small fluctuations in the estimation process, and finally converges around the set value of 0.3. The maximum estimation error of the road adhesion coefficient is 0.01, which has a good estimation effect. The vehicle speed of 55 km/h at the longitudinal position of 35m-50m is selected as the boundary of the centroid sideslip angle-the centroid sideslip angular velocity phase plane. The vehicle trajectory curves of the three groups of controllers are almost all within the boundary curve, and the vehicle is in a stable state. Therefore, under the low adhesion coefficient road surface, if the prediction horizon is too small, the trajectory tracking control effect will be deteriorated. The adaptive prediction horizon adjustment effect is not obvious, and the trajectory tracking control effect of controller A and controller B is close.

VI. CONCLUSION

In this article, the problem of trajectory tracking control of driverless racing car under extreme conditions is addressed, while ensuring its stability and tracking accuracy. A trajectory tracking control strategy is proposed, and the controller is designed based on the proposed control strategy. Validated by co-simulation with MATLAB/Simulink and CarSim. The results show that the trajectory tracking control strategy proposed in this article can consider the vehicle stability and trajectory tracking accuracy under the extreme conditions of high-speed turning with different road adhesion coefficients.

In future work, we will carry out hardware-in-the-loop experiments to verify the control strategy on the hardware-in-the-loop test bench to test the feasibility of the algorithm on the test bench. In addition, we will improve the road adhesion coefficient estimation algorithm. The estimation algorithm based on tire force used in this article has a certain error in the road adhesion coefficient estimation when the tire force changes greatly. Meanwhile, we will study the use

of advanced control methods in this system to improve the control accuracy.

REFERENCES

[1] C. Hu, R. Wang, F. Yan, Y. Huang, H. Wang, and C. Wei, "Differential steering based yaw stabilization using ISMC for independently actuated electric vehicles," *IEEE Trans. Intell. Transp. Syst.*, vol. 19, no. 2, pp. 627–638, Feb. 2018.

[2] L. Xiong, X. Yang, G. Zhuo, B. Leng, and R. Zhang, "Review on motion control of autonomous vehicles," *J. Mech. Eng.*, vol. 56, no. 10, pp. 143–159, Apr. 2020.

[3] M. Gerdts, S. Karrenberg, B. Müller-Beßler, and G. Stock, "Generating locally optimal trajectories for an automatically driven car," *Optim. Eng.*, vol. 10, no. 4, pp. 439–463, Apr. 2008.

[4] E. Velenis and P. Tsiotras, "Minimum-time travel for a vehicle with acceleration limits: Theoretical analysis and receding-horizon implementation," *J. Optim. Theory Appl.*, vol. 138, no. 2, pp. 275–296, 2008.

[5] L. Cardamone, D. Loiacono, P. L. Lanzi, and A. P. Bardelli, "Searching for the optimal racing line using genetic algorithms," in *Proc. IEEE Conf. Comput. Intell. Games*, Aug. 2010, pp. 388–394.

[6] P. A. Theodosis and J. C. Gerdes, "Nonlinear optimization of a racing line for an autonomous racecar using professional driving techniques," in *Proc. Adapt. Control; Adv. Vehicle Propuls. Syst.; Aerosp. Syst.; Auto. Syst.; Battery Modeling; Biochem. Syst.; Control Over Netw.; Control Syst. Design; Cooperativ*, vol. 1, Oct. 2012, pp. 235–241.

[7] D. Casanova, R. S. Sharp, and P. Symonds, "Minimum time manoeuvring: The significance of yaw inertia," *Vehicle Syst. Dyn.*, vol. 34, no. 2, pp. 77–115, Aug. 2000.

[8] C. G. Bobier and J. C. Gerdes, "Staying within the nullcline boundary for vehicle envelope control using a sliding surface," *Veh. Syst. Dyn.*, vol. 51, no. 2, pp. 199–217, 2013.

[9] N. R. Kapania and J. C. Gerdes, "Design of a feedback-feedforward steering controller for accurate path tracking and stability at the limits of handling," *Vehicle Syst. Dyn.*, vol. 53, no. 12, pp. 1687–1704, Dec. 2015.

[10] S. M. Erlien, S. Fujita, and J. C. Gerdes, "Safe driving envelopes for shared control of ground vehicles," *IFAC Proc. Volumes*, vol. 46, no. 21, pp. 831–836, 2013.

[11] N. R. Kapania and J. C. Gerdes, "Path tracking of highly dynamic autonomous vehicle trajectories via iterative learning control," in *Proc. Amer. Control Conf. (ACC)*, Jul. 2015, pp. 2753–2758.

[12] T. Novi, A. Liniger, R. Capitani, and C. Annicchiarico, "Real-time control for at-limit handling driving on a predefined path," *Vehicle Syst. Dyn.*, vol. 58, no. 7, pp. 1007–1036, Jul. 2020.

[13] Y. Wang, S. Gao, Y. Wang, Y. Xu, D. Guo, and Y. Zhou, "Trajectory tracking and stability control of high-speed autonomous vehicle," *J. Zhejiang Univ. Eng. Sci.*, vol. 55, no. 10, pp. 1922–1929, Oct. 2013.

[14] H. Jin and S. J. Li, "A research on vehicle stability control based on limited speed," *Automot. Eng.*, vol. 40, no. 1, pp. 48–56, 2018.

[15] S. Li, K. Guo, T. Chou, H. Chen, G. Wang, and G. Cui, "Stability control of vehicle with active front steering under extreme conditions," *Automot. Eng.*, vol. 42, no. 2, pp. 191–198, Mar. 2020.

[16] L. Chen, Y. Xie, Y. Cai, X. Sun, C. Teng, and K. Zou, "Stable tracking control of autonomous vehicles at extreme conditions," *Automot. Eng.*, vol. 42, no. 8, pp. 1016–1026, Aug. 2020.

[17] Z. Xin, H. Chen, Z. Lin, E. Sun, Q. Sun, and S. Li, "Lateral trajectory following for automated vehicles at handling limits," *J. Mech. Eng.*, vol. 56, no. 14, pp. 138–145, Jul. 2020.

[18] C. Sun, X. Zhang, L. Xi, and H. Chen, "Design for the steering controller of autonomous vehicles at the limits of handling," *J. South China Univ. Technol. Natural Sci. Ed.*, vol. 46, no. 3, pp. 78–85, Mar. 2018.

[19] L. Fang, L. Ma, S. Ding, and J. H. Park, "Finite-time stabilization of high-order stochastic nonlinear systems with asymmetric output constraints," *IEEE Trans. Syst., Man, Cybern. Syst.*, vol. 51, no. 11, pp. 7201–7213, Nov. 2021.

[20] L. Fang, S. Ding, J. H. Park, and L. Ma, "Adaptive fuzzy control for non-triangular stochastic high-order nonlinear systems subject to asymmetric output constraints," *IEEE Trans. Cybern.*, vol. 52, no. 2, pp. 1280–1291, Feb. 2022.

[21] L. Liu, S. Ding, and X. Yu, "Second-order sliding mode control design subject to an asymmetric output constraint," *IEEE Trans. Circuits Syst. II, Exp. Briefs*, vol. 68, no. 4, pp. 1278–1282, Apr. 2021.

[22] L. Liu, W. X. Zheng, and S. Ding, "An adaptive SOSM controller design by using a sliding-mode-based filter and its application to buck converter," *IEEE Trans. Circuits Syst. I, Reg. Papers*, vol. 67, no. 7, pp. 2409–2418, Jul. 2020.

[23] C. Bardawil, R. Talj, C. Francis, A. Charara, and M. Doumiati, "Integrated vehicle lateral stability control with different coordination strategies between active steering and differential braking," in *Proc. 17th Int. IEEE Conf. Intell. Transp. Syst. (ITSC)*, Oct. 2014, pp. 314–319.

[24] T. Chung and K. Yi, "Design and evaluation of side slip angle-based vehicle stability control scheme on a virtual test track," *IEEE Trans. Control Syst. Technol.*, vol. 14, no. 2, pp. 224–234, Mar. 2006.

[25] B.-C. Chen, C.-T. Tsai, and K. Lee, "Path-following steering controller of automated lane change system with adaptive preview time," in *Proc. IEEE Int. Conf. Syst., Man, Cybern.*, Oct. 2015, pp. 2522–2526.

[26] B. Zhang, "Trajectory tracking control research on full X-by-wire electric vehicle based on different maneuvering modes," Ph.D. dissertation, School Automot. Eng., Jilin Univ., Jinlin, China, 2020.

SUCAI ZHANG is currently pursuing the degree with the Liaoning University of Technology.

He has authored or coauthored four journals and conference papers. He has authorized one utility model patent. His current research interest includes simulation and intelligent control for vehicle.

GANG LI received the M.S. degree in vehicle engineering from the Liaoning University of Technology, Jinzhou, China, in 2006, and the Ph.D. degree from Jilin University, Changchun, China, in 2013.

He is currently a Professor and the Dean of the College of Automobile and Traffic Engineering, Liaoning University of Technology. He is in charge of the projects funded by the national government and institutional organizations on electric vehicles and energy management systems. He has authored or coauthored more than 50 journals and conference papers. He was a recipient of 30 China patents and software copyrights. His current research interests include model, simulation, and intelligent control for vehicle, and vehicle active safety.

LIYONG WANG received the M.S. degree in vehicle engineering from Chongqing University, Chongqing, China, in 2005, and the Ph.D. degree in vehicle engineering from the Beijing Institute of Technology, Beijing, China, in 2008.

He is currently a Professor and the Dean of the Beijing Key Laboratory of Measurement and Control of Mechanical and Electrical System Technology, Beijing Information Science and Technology University. He has successively in charge of over more than 20 national, provincial, and national defense projects, and published more than 100 articles. His current research interests include intelligent vehicle control and intelligent operation and maintenance, electromechanical system condition monitoring, and fault diagnosis technology research.